
Sea Ice Modelling and Forecasting

Sylvain Bouillon, Pierre Rampal, and Einar Olason

Nansen Environmental and Remote Sensing Center, Bergen, Norway

Sea ice is a fascinating media, of which modelling is in its infancy compared to the ocean and atmosphere. This chapter focuses on the new frontiers in sea ice modelling and forecasting, with particular attention on sea ice dynamics. It is divided in two sections: 1) New frontiers in sea ice modelling and 2) New frontiers in sea ice forecasting. In the first section, we describe ice pack dynamics and then concentrate on the representation of sea ice dynamics in continuous models. A sub-section discusses the potential impacts on the ocean and atmosphere of explicitly resolving some features related to sea ice dynamics, in particular the opening and closing of leads, in coupled modelling systems. In the second section, we point out three important constraints on sea ice forecasting related to 1) potentially large biases in the near real-time data, 2) time-varying biases in the external forcing, and 3) far-from-equilibrium dynamical state. These points are explored by addressing the two following questions: "How can we beat ice charts persistency?" and "Can we predict sea ice fracturing and deformation days in advance?"

New Frontiers in Sea Ice Modelling

First, we describe sea ice and how the intrinsic properties of this material result in a complex dynamical behavior that is different from geophysical turbulent fluids such as the ocean and the atmosphere. We also highlight the similarities and differences between the mesoscale dynamical features present in the atmosphere (synoptic features), the ocean (eddies), and the sea ice pack (linear kinematics features), as well as some important interactions that exist between the ice cover dynamical system and the two other systems.

Then we make an attempt to define a unified modelling framework for reproducing the observed ice pack dynamics. This is achieved by combining ingredients taken from the first-generation dynamical models introduced in the 1970s (Hibler, 1979), which are still dominantly used today, with new approaches recently proposed to explicitly resolve the kinematic features (faults, ridges, and leads) present in the ice pack. This framework is in some ways the counterpart of that used in oceanography to classify models into laminar, eddy-permitting, and eddy-resolving implementations.

A unified framework, taking into account the resolved and unresolved scales, may be crucial to rethink most of the parameterizations used in sea ice modelling to date. Such a framework will likely require some adaptation of the coupling strategies that have been developed to connect the sea ice with the ocean underneath and the overlying atmosphere. Along those lines, we will wrap

Bouillon, S., P. Rampal, and E. Olason, 2018: Sea ice modelling and forecasting. In "New Frontiers in Operational Oceanography", E. Chassignet, A. Pascual, J. Tintoré, and J. Verron, Eds., GODAE OceanView, 423-444, doi:10.17125/gov2018.ch15.

up this section by looking at how sea ice lead fraction can be simulated by a next generation sea ice model and how it may impact the representation of the ocean-atmosphere interactions.

Sea ice and ice pack dynamics

The term “sea ice” is used to designate all types of ice coming from freezing sea water. Sea ice formation starts with frazil ice formation. During this process, a large amount of salt is released into the underneath water column, while some remains trapped in the ice as brine pockets. Those pockets are being emptied over time by a drainage/percolation process of the brines through the ice, allowing the ice cover to become similar to fresh ice within a couple of months. Ice growth continues through processes such as pancake formation, rafting, ridging, and consolidation, the occurrence of which depends on oceanic conditions (calm or agitated). Finally, this sometimes leads to the formation of a nearly continuous sheet of ice a few meters thick that floats on top of the ocean, extending over thousands of kilometers; this is commonly called the “sea ice pack” or “sea ice cover.” A sea ice pack should not be confused with the ice sheets or ice shelves made from freshwater ice formed by a slow compaction process of snow and typically from hundreds to thousands of meters thick.

The “pack ice” (ice composing the sea ice pack) is an efficient insulator, especially when snow is present on top (e.g., Maykut et al., 1986; Andreas et al., 1979). A snow-covered, non-moving continuous ice pack drastically reduces the exchanges of heat, water, and momentum between the ocean and atmosphere, and it strongly limits long- and short-wave radiation transfers.

The simplest model for a snow-covered, non-moving continuous ice pack could be based on a 0-layer vertical heat transfer model and it would have only two prognostic variables, the snow and ice thicknesses. More complex models would consider a larger number of vertical layers in the snow and ice, with prognostic variables for the temperature and salinity in each layer, and a fine representation of snow metamorphism and upper surface processes (e.g., the formation of melt ponds).

In nature, however, the sea ice pack is not made of a continuous sheet of ice with homogeneous thickness; instead, it is highly fractured and exhibits a chaotic surface that combines pressure ridges, open leads, and plates of intact “level ice” in between. The ocean-atmosphere heat fluxes are typically much larger for open water and thin ice than for thick ice, meaning that fluxes through the leads make a large contribution to the total energy transfer even if they cover only a small percentage of the total ice pack area (see, for example, Lupkes et al., 2008a; 2008b; Marcq and Weiss, 2012; Vihma et al., 2013 for a review). In winter, this transfer corresponds to an intense and highly local injection of heat and moisture into the atmosphere, as well as formation of new ice tied to the release of large amounts of salt into the upper ocean. Ridges and leads define surface and bottom roughness, and therefore drastically affect surface and bottom stresses acting at the ice-atmosphere and ice-ocean interfaces due to the action of winds and currents.

Why does the ice pack not simply deform homogeneously as a pure linear elastic media or as a highly viscous fluid? The quick answer is because sea ice is a solid, brittle material. Under forces load, the ice pack only deforms elastically below a given critical internal stress (corresponding to the range of infinitesimal–non permanent deformation), breaks into pieces along fractures when this

critical stress is reached, and then eventually continues to deform if large-scale forces are still applied (corresponding to large-scale permanent deformation), with energy dissipation at the edges of those pieces that is related to friction mechanism.

There are multiple driving forces for breaking the ice. Thermal cracking is observed when rapid and large variations of temperature occur in the vertical dimension (Weeks et al., 2010, chapter 10.4). Ice can also break due to vertical load, which is the technique used by icebreakers to progress in areas covered by high concentrations of ice (Bazant, 2000). In the marginal ice zone (i.e., the transition area between the open ocean and the pack ice), the dominant process that breaks the ice is the flexural bending due to ocean surface waves. However, the dominant cause overall for sea ice breaking, particularly in the central Arctic, is the presence of spatial gradients in the wind and ocean stresses acting on the ice.

Breaking generates blocks of ice with length scales from a few meters to hundreds of meters depending on the driving force involved (tides, waves, eddies, atmospheric features...). Based on the surrounding conditions, these blocks may be pushed against each other to form ridges that are typically tens of meters thick, further broken into smaller pieces (typically when enduring shear deformation), or moved apart to reveal open water areas between blocks. The breaking of the ice and the subsequent collisions and friction between the blocks generates large energy dissipation. Some part of the kinetic energy is also transformed into potential energy due to the build-up of ridges. Numerical simulations with discrete models (Hopkins et al., 1991) and analyses of in situ observations have yielded a solid knowledge of the ridging process at the scale of an individual ridge. As discussed in detail later in this chapter, it will be important to take those local processes into account when building a sea ice model for the ice pack.

It is only since the late 1990s, with the implementation of automated sea ice drift estimation from the synthetic-aperture radar images retrieved by RADARSAT (Kwok et al., 1990), that sea ice scientists began to get sufficient amounts of observations, both in terms of coverage and resolution in the temporal and spatial domain, to really understand the mechanisms controlling sea ice dynamics. From the sea ice drift Radarsat Geophysical Processor System (RGPS) dataset, one can derive sea ice deformation fields at a resolution of 10 km and three days over the whole Central Arctic and for an entire season. A first look at these deformation fields (see example in Fig. 15.1, first panel) reveals that most of the deformation is localized along linear features while the rest of the ice pack exhibits no or little deformation, mimicking the plate tectonic of the Earth crust characterized by fracturing processes and faulting mechanism. Those linear kinematics features can be hundreds of kilometers long and appear to be organized into systems of nearly parallel lines. New linear kinematics features are formed very quickly (much faster than three days, which is the temporal resolution of the RGPS data) and they are generally aligned with the atmospheric isobars, meaning that they are, at the time of their “activation,” perpendicular to the gradient in the wind stress. These networks of fractures typically have a persistence of several weeks, during which the same set of linear kinematics features remain active. This long persistence, compared to the synoptic scale, is attributed to the fact that once sea ice is fractured and a linear feature is formed, it represents a much weaker zone in the ice pack that will likely accommodate large shear deformation. Shear

deformation is also associated with large values of divergence and convergence, corresponding to leads opening and ridges building. Changes from one linear kinematics feature's system to another one can happen when the ice has recovered enough of its mechanical strength due to ice refreezing in cracks or leads or ridge consolidation, so that a next external forcing will generate another set of linear kinematics features with different directions (see discussion and images in Kwok, 2001).

Complex systems with dynamics controlled by highly localized extreme events can be analyzed quantitatively by performing scaling analysis, i.e., by looking at how statistical distributions change with the scale of observation. Fig. 15.1 shows the result of a coarse graining procedure where deformation is computed at different scales, from 7 to 200 km. It is important to note that some linear features are still visible at scales as large as 100 km, invalidating the homogenization methods on which continuous models are generally based. That is an issue we will discuss in greater detail later in this chapter.

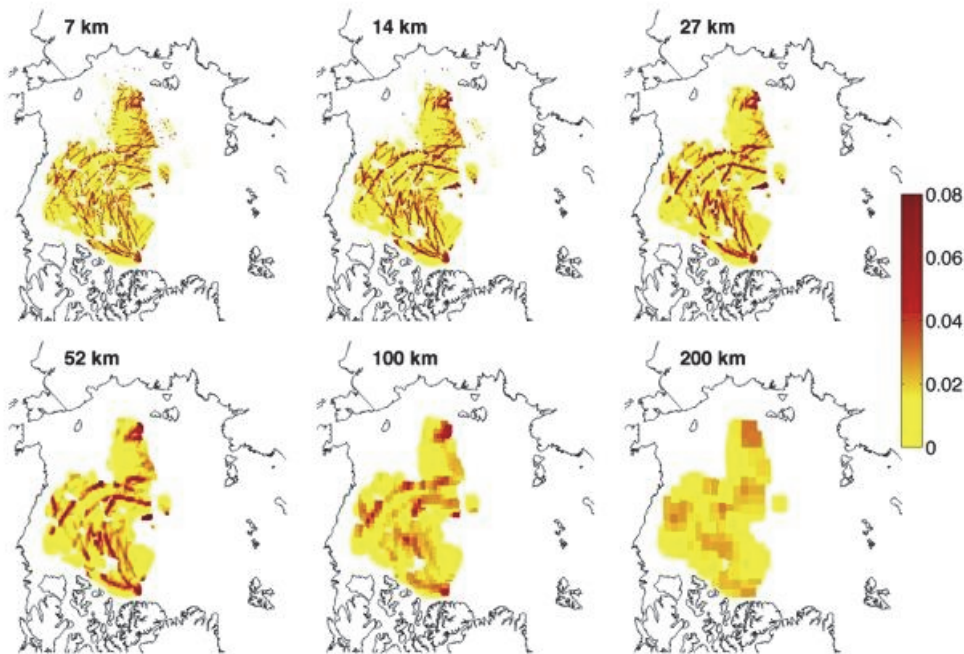


Figure 15.1. Shear rates [in one/day] computed from 3-days ice drift from the RGPS dataset at spatial scales of 7 to 200 km over the Central Arctic.

Scaling analysis of sea ice deformation can also be computed by looking at the dispersion of pairs of drifting buoys (either real buoys set in the ice or virtual buoys from a model or from the RGPS trajectories). As the same pairs of buoys can generally be followed for long periods of time, using dispersion analysis allows us to look at the temporal scaling, i.e., how the statistical distributions depend on the timescale of observation. From the RGPS trajectories dataset (see example in Fig. 15.2), we can define many pairs of buoys with initial separation $L(0)$ ranging from 10 km to hundreds of kilometers. A proxy of the deformation rate can then be defined as

$$\dot{\epsilon} = \frac{L(t) - L(t-T)}{L(t) T} \quad (1)$$

with T defining the temporal scale of observation.

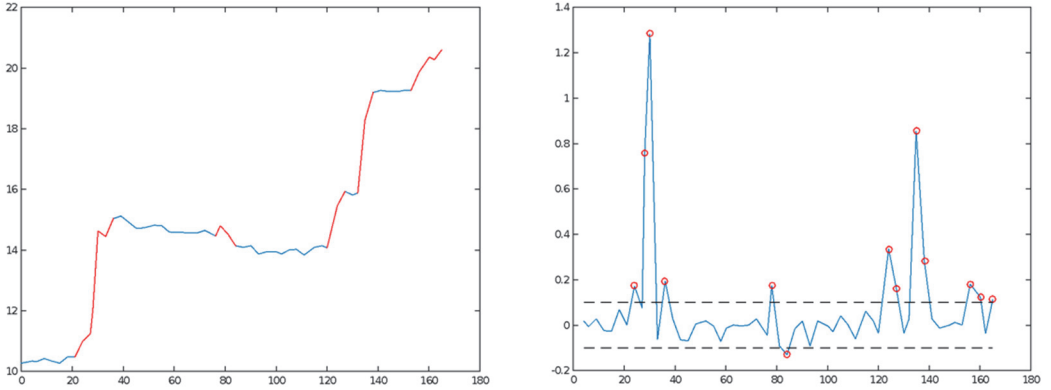


Figure 15.2. Separation [in km] and separation rate [in km/day] for a pair of RGPS trajectories followed for about 160 days in winter 2006-07. The section and circles in red indicate the deformation events when the separation rate is larger than 100 m per day.

Power-law scaling in space is observed for the moments of the distribution,

$$\langle \dot{\varepsilon}^q \rangle_{L,T} \sim L^{-\beta(q)} \quad (2)$$

with two different structure functions $\beta(q)$, one for $L \leq 100$ km and another for $L \geq 100$ km (Fig. 15.3). The analysis of different buoy trajectory datasets (Rampal et al., 2008; Hutchings and Hibler, 2008; Hutchings et al. 2011) shows that the scaling obtained from the analysis of the RGPS data holds for much smaller scales of about hundreds of meters. Some authors suggested that it may hold down to the scale of one meter (Marsan et al., 2004), which is the typical thickness of the ice pack where energy can be largely dissipated when ridges are formed or shear faulting occurs.

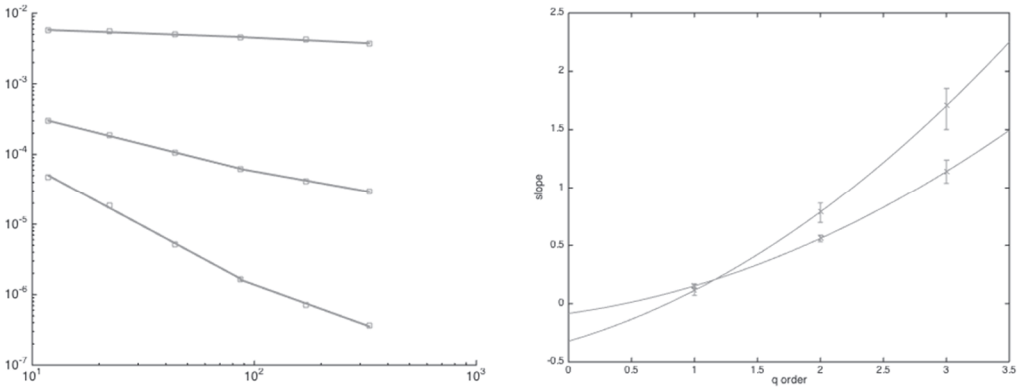


Figure 15.3. Spatial scaling analysis of the deformation for spatial scales ranging from $L=10$ km to $L=350$ km. On the left panel, the first (upper curve, $q=1$), second (middle curve, $q=2$) and third (lower curve, $q=3$) order moments of the distributions [in one/day] are plotted against the scale L of observation [in km]. A cut in the scaling is observed at $L=100$ km. On the right panel the structure function $\beta(q)$ is plotted for $L \leq 100$ km and $L \geq 100$ km.

Based on the assumption that the scaling laws remain valid for smaller scales and using the information on the structure function $\beta(q)$ for $L \leq 100$ km, one can actually extrapolate the probability density functions of our proxy of the deformation to smaller scales by using the method proposed in Marsan et al. (2004). Fig. 15.4 shows that the probability density functions seamlessly

transition from an exponential (straight line in the semilog axis, right panel) to a power law (straight line in the loglog axis, left panel) when going towards smaller scales of observation. Such extrapolation towards the smallest scale (1.25 km, in our example) leads to a probability density function that is very close to a power law with an exponent k close to 2 and a multiplicative factor $C=0.005$

$$\lim_{L \rightarrow 1m} p(\dot{\epsilon}) = C \dot{\epsilon}^{-k} \tag{3}$$

Power law distributions with an exponent k close to 2 are typical of systems where the whole distribution is dominated by extreme values. For $k \leq 2$, even the mean becomes infinite.

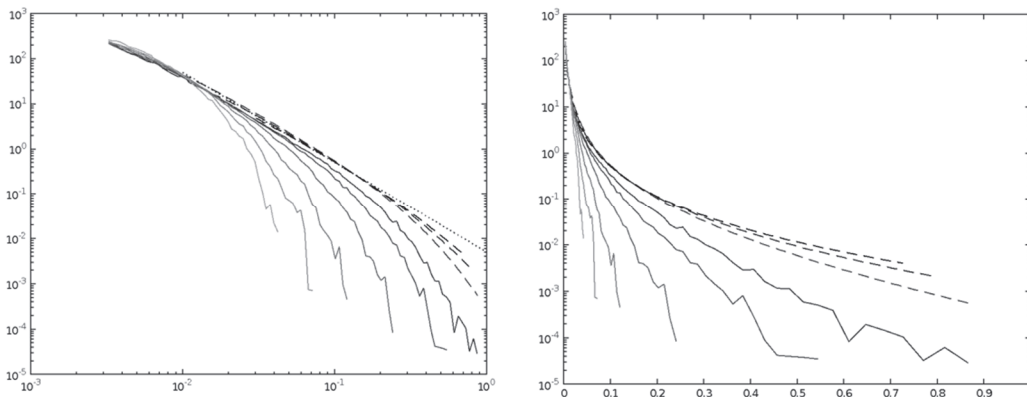


Figure 15.4. Probability density functions of the deformation rate computed at $T=3$ days and for L going from 360 to 10 km (solid lines from gray to dark gray) and extrapolated for $L=5, 2.5$ and 1.25 km (dashed line from gray to black), in a loglog plot (left) and a semi-log plot (right). The power law function $C \dot{\epsilon}^{-k}$ with $C=0.005$ and $k=2$ is plotted as a dotted line for reference.

However, in nature distributions exhibit cut-off for very large values. In the case of sea ice, one could, for example, propose an exponential cutoff so that the deformation rate probability density function at scale L would have the following shape:

$$p_L(\dot{\epsilon}) = C \dot{\epsilon}^{-k} e^{-\lambda(L)\dot{\epsilon}} \tag{4}$$

where $\lambda(L)$ is a positive monotonically increasing function of the spatial scale of observation. Preliminary test showed that $\lambda(L) = L$ is a good first estimate (not shown). Note that the numbers given here are for L in km and $\dot{\epsilon}$ in one/day.

The scaling analysis can also be performed for the temporal domain. As for the spatial domain, power law scaling is observed for the different moments (here with $q=0.5$ to $q=3$):

$$\langle \dot{\epsilon}^q \rangle_{L,T} \sim T^{-\alpha(q)} \tag{5}$$

The structure function $\alpha(q)$, defining how the moments of the distribution varies as a function of the time scale of observation, is different for scales shorter than \sim ten days and longer than \sim ten days (see Figure 15.5). This change in the scaling around ten days corresponds to the typical time interval between two successive synoptic atmospheric events. Probability density functions could also be extrapolated to time scales lower than 3 days (not done here) by using the structure functions $\alpha(q)$.

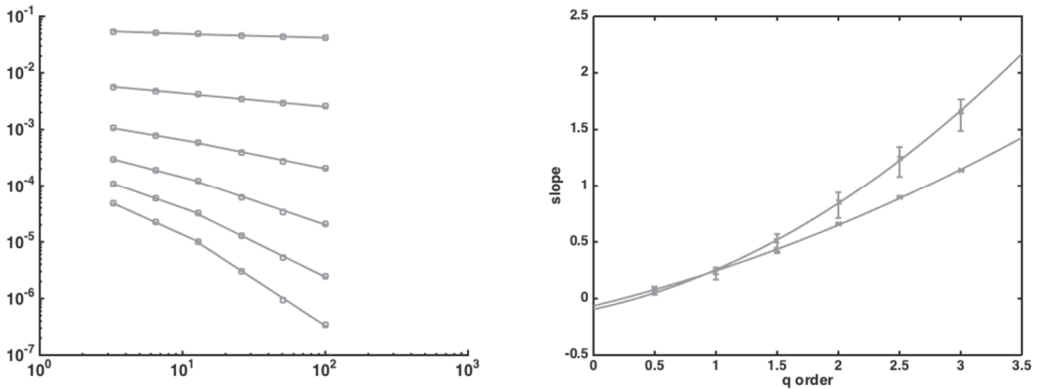


Figure 15.5. Temporal scaling analysis of the deformation rates [in 1/day] for temporal scales ranging from $T=3$ days to $T=100$ days. On the left panel, the first (upper curve), second (middle curve) and third (lower curve) order moments of the distribution are plotted against the temporal scale T of observation. A cut in the scaling is observed at $T=10$ days. On the right panel the structure function $\beta(q)$ is plotted for $T \leq 10$ days and $T \geq 10$ days.

Taking into account the observed temporal and spatial scaling of sea ice deformation is crucial to make the link between the scales at which the energy is introduced in the system (synoptic scales, ten days, hundreds of kilometers) and the scales at which it is dissipated by breaking the ice and building ridges (dissipation scale, a few hours, 1-10 m). Making this connection is at the basis of the unified modelling framework developed recently and described below.

A unified modelling framework for the ice pack

As discussed in the previous section, sea ice dynamics have many similarities with plate tectonics and earthquakes physics, but at much smaller temporal and spatial scales. The ice pack dynamics are controlled by intermittent and highly localized shearing events accommodating a large part of sea ice deformation and energy dissipation. Simulating such complex dynamics is a challenge that has still not been completely achieved. In this subsection, we briefly describe the components and results of the first generation dynamical models for sea ice, which were mainly developed to simulate the large-scale sea ice circulation. We also present a new modelling framework that takes into account the links between scales described previously.

Like the ocean and the atmosphere, the ice pack is subject to large-scale circulations, characterized in the Arctic by the Beaufort gyre and the transpolar drift, and around Antarctica by the Antarctic coastal (westward) and circumpolar (eastward) currents. For the Central Arctic, these currents have typical time- and length-scales of about 5-6 months and 400 km for winter and 2-3 months and 200 km for summer. The seasonal and interannual variability of these currents are largely controlled by the change in the sea ice extent and volume, as well as by the seasonal and interannual variability of the atmosphere and ocean. The amplified effects of climate change in polar regions also affect the trends in the large-scale circulation (Rampal et al., 2009).

The first dynamical models of sea ice were built to reproduce the large-scale circulation of sea ice. At these scales, the momentum equation basically resumes to the equilibrium between three forces: the surface stress from the wind (τ_a), the surface stress from the ocean current (τ_w), and the

gradient of the internal stress integrated on the vertical. Different parameterizations for the air-ice and water-ice surface stresses are used, the simplest being that the surface stresses depend linearly on the difference between the horizontal ice velocity u and the horizontal air velocity u_a and water velocity u_w , respectively. The simplest surface stress parameterizations also neglect the turning angle and assume that ice speed is much lower than air speed, leading to the following equation for the momentum balance:

$$0 = \rho_a c_a u_a + \rho_w c_w (u_w - u) + \nabla \cdot (\sigma H) \quad (6)$$

where ρ_a and ρ_w are the air and water densities, c_a and c_w are the air and water drag coefficients for sea ice, H is the ice “thickness” (volume per unit area), and σ is the internal stress tensor.

A rheological model is needed to define the link between the deformation and internal stress. The model dominantly used is based on a plastic rheology, where the internal stress in shear and convergence depends solely on the sea ice thickness and mode of deformation. In one dimension, the plastic rheology gives a constant value $\sigma_I = -P$ when the divergence rate is negative or null, and $\sigma_I = 0$ otherwise.

The momentum equation is coupled to the volume conservation equation:

$$\frac{\partial H}{\partial t} = -\nabla \cdot (uH) + f_H \quad (7)$$

where f_H is a sink/source term related to thermodynamics. For a simple case with no thermodynamics, no ocean currents, and where the ice is pushed towards the coast with a constant wind velocity, the stationary solution corresponds to a zero velocity and a linear function for the thickness field with a slope $\frac{\partial H}{\partial x} = \frac{\tau_a}{P}$. The ice strength parameter P then defines the large scale thickness gradient. When sea ice is diverging, the internal stress is zero and the ice moves in free drift mode with a velocity set by:

$$u = \frac{\rho_a c_a}{\rho_w c_w} u_a + u_w \quad (8)$$

The ratio $\frac{\rho_a c_a}{\rho_w c_w}$ is the Nansen number that was first estimated by the Norwegian Fridtjof Nansen when comparing the drift of his boat (the Fram) trapped in the ice with the wind speed.

Such a model, with only the volume per unit area and the horizontal ice velocity as variables, is rarely used because it is important to know the sub-grid scale distribution of the ice thickness to correctly represent some processes, particularly the processes related to thermodynamics. To do so, one defines a thickness distribution $g(h)$ within each cell that has the following properties:

$$\int_0^\infty g(h) dh = 1 \quad (9)$$

and

$$\int_0^\infty g(h) h dh = H. \quad (10)$$

The governing equation for the thickness distribution is:

$$\frac{\partial g}{\partial t} = -\nabla \cdot (ug) - \frac{\partial}{\partial t} (fg) + \psi \quad (11)$$

where $f(h)$ is a sink/source term from the thermodynamics (equivalent to an advection term in the thickness space), and ψ is a redistribution term that transfers sea ice from one thickness to another. The following constraints on the redistribution term:

$$\int_0^\infty \psi dh = \nabla \cdot u \quad (12)$$

and

$$\int_0^\infty h \psi dh = 0 \quad (13)$$

are obtained to respect equations (11) and (9). In practice all sea ice models consider a sub grid scale thickness distribution of the ice. Multi-category models usually define it using N distinct categories:

$$g(h) = \sum_{i=0}^{N-1} a_i \delta(h - h_i) \quad (14)$$

with $h_0 = 0$ for the open water and $\delta(h)$ a Dirac delta function, the simplest being the two-category ice thickness distribution where only two prognostic variables, the ice concentration a_1 and the ice thickness h_1 , and where $h_0 = 0$ and $a_0 = 1 - a_1$. Other representation of the ice thickness distribution may be defined based on observations using, for example, modal analyses that often show one mode for open water, one for refrozen leads, and one for level – non deformed ice and a negative exponential tail for the ridged ice.

Whatever the representation of the thickness distribution, one needs to define the redistribution term ψ in eq. 11. The framework to define the redistribution term was established by Thorndike (1975). The scheme is based on many assumptions that will not be listed here, but the main underlying assumption is that one needs to define a subgrid-scale distribution of the ice deformation because the deformation at the scale of one model cell will not correspond to the deformation at the scale of one lead or ridge. This is well-illustrated in Fig. 15.6, extracted from Thorndike (1975), which shows a case with no divergence at the scale of the grid cell, but with some local ridging and lead opening. The redistribution scheme proposed by Thorndike is actually equivalent to integrating a ridging model (given the evolution of the thickness at the scale of a single ridge and lead) over a subgrid-scale distribution of the ice deformation. In Thorndike (1975), the ridging model is very simple and supposes that when a ridge is formed its thickness is k times the thickness of the surrounded ice, with k set to 5. The formation of a ridge then corresponds to the redistribution process $\gamma(h_1, h_2) = \frac{1}{k} \delta(h_2 - kh_1)$.

A more complete redistribution scheme has recently been proposed to take into account the evolution of the macro-porosity (holes between ice blocks, see the presentation of A. Roberts at the Newton Institute, <https://www.newton.ac.uk/seminar/20170913094510301>). Such a model makes a consistent link with the ridging processes occurring at the scale of the ridges, and also estimates correctly the distributions of ridge separation, thickness, and shape.

The redistribution process is a key component in sea ice models as it makes room for open water areas through which a large amount of heat, momentum, and mass can be exchanged between the ocean and the atmosphere. It is also a way to make a consistent link between the energy dissipated and the work done during the ridging process and the energy extracted by the rheological term. In

most sea ice models, however, this link is simply not made, and when it is accounted for, it is usually based on simplistic approaches where the energy dissipation is simply scaled as a constant (about 15-20) of the increase in potential energy due to ridging. The approach recently presented by Roberts tackles this issue and provides a more sound representation of the energy dissipation and work done during the ridging process.

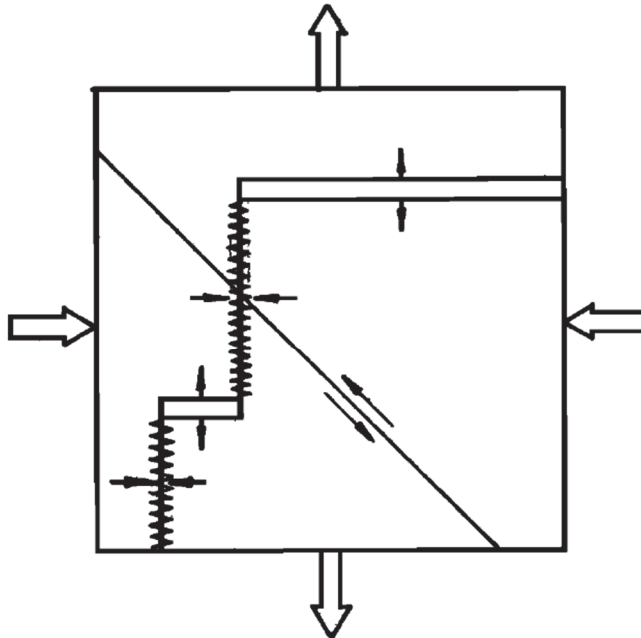


Fig. 10. Schematic diagram illustrating the formation of leads and pressure ridges during pure shearing deformation.

Figure 15.6. From Thorndike (1975; Fig. 10) illustrating the ridging scheme.

Another important assumption when defining any redistribution schemes is that the sea ice model simulates correctly the shear and divergence rate at the scale of the model cells. Knowing that below 100 km the deformation is highly localized, the rheology used for continuous models running at spatial scales smaller than 100 km ($\Delta x < 100 \text{ km}$) must then allow localization of the deformation at the scale of one model cell. A solution that has been proposed is to add a large-scale variable, referred to as the local damage of sea ice and defined at the scale of one model cell (i.e., for a 10 km x 10 km or a 100 km by 100 km cell). The ice damage is set to range between zero (for intact ice pack) and one (for totally damaged ice pack). A proposed model that includes a damage variable is the Maxwell-Elasto-Brittle (Maxwell-EB) rheology (Dansereau et al., 2016). In this model, the internal stress builds up as an elastic medium for undamaged ice. If the ice stress reaches a defined stress envelope, it fails, meaning that the damage increases and a viscous relaxation term is activated so that the accumulated stress is rapidly damped out. While the ice cell remains damaged, it can accommodate large deformation. The model assumes that the damage can be reduced via some healing processes, so that after typically several days or weeks, this cell is able to accumulate internal stress and mechanically resist external forces again. The Maxwell-EB rheology has been implemented in the finite element sea ice model neXtSIM (Bouillon and Rampal, 2015;

Rampal et al., 2016a) and used successfully to reproduce the scaling laws described previously down to the model resolution (Rampal et al., 2017). Fig. 15.7 shows an example of the sea ice drift and deformation simulated by the neXtSIM model, with localization of the deformation at the scale of the model grid cell, meaning discontinuities in the velocity field. Such a model is still continuous but it is able to generate a discrete-like behavior in which one can identify individual ice plates, moving like solid bodies and surrounded by areas of high deformation.

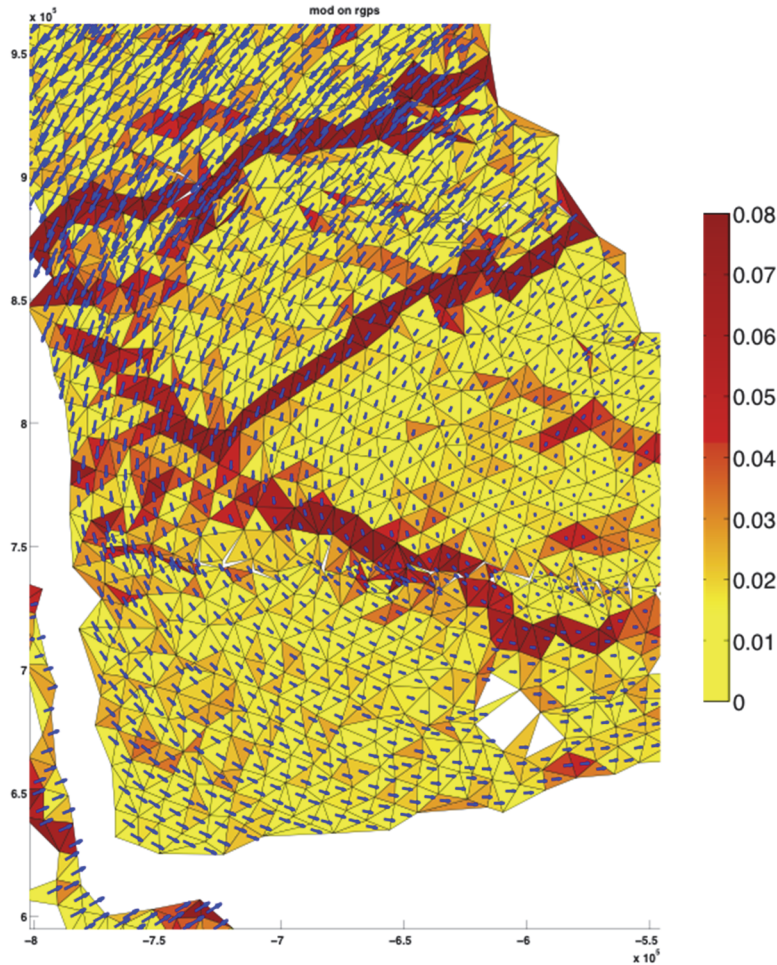


Figure 15.7. Sea ice drift and deformation simulated by the Maxwell-Elasto-Brittle model running at a resolution of 10 km and plotted as if it was computed with the RGPS system, meaning at a resolution of about 10 km and with a time interval of three days.

A model that allows strain localization will also produce sharp variations for scalar quantities such as the thickness and concentration fields. Having an advection scheme that is able to transport such sharp gradients without degrading them is a challenge for classical Eulerian advection schemes applied on a fixed grid and where advection corresponds to computing fluxes through the element's edges. An alternative is to use a Lagrangian framework where the model grid moves with the ice (see Fig. 15.8). Such an advection scheme has been implemented in the neXtSIM model (Samaké et al., 2017).

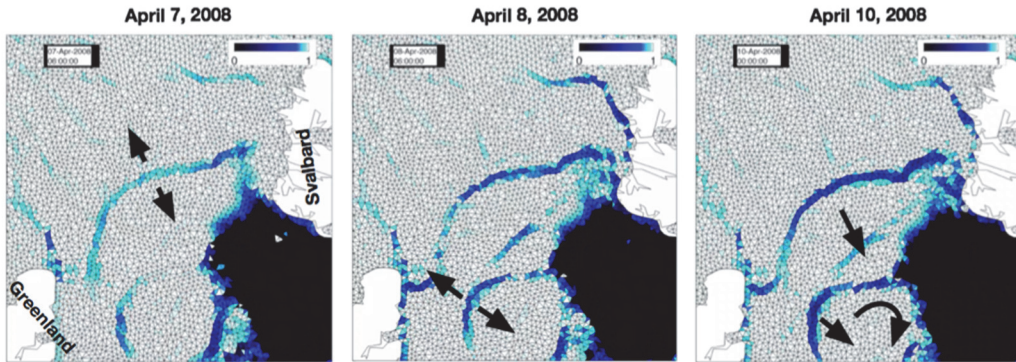


Figure 15.8. Example of sea ice concentration fields at Fram Strait and the underlying moving mesh coming from a one-year simulation using neXtSIM in a full Arctic configuration and with a resolution of about 10 km. The maps show how the localized divergence generates discontinuities in the ice cover at the scale of the mesh resolution and how these discontinuities are preserved over time by the Lagrangian advection scheme. Figure from Samaké et al. (2017).

A unified framework for continuous sea ice dynamics model running at resolutions from 0.1 to 100 km would then consist of the following:

- the momentum equation,
- a rheological model able to localise the deformation at the scale of one model cell,
- an advection scheme able to transport ice field without degrading their spatial localisation,
- a redistribution scheme making the link between the deformation at the scale of the model cells and the subgrid-scale ridging processes.

Implementing such a framework has not been completely achieved yet, because all of the above ingredients need to be present at the same time. For example, it was shown that classical viscous-plastic rheology with multi-category ice thickness distribution and energy consistent redistribution schemes perform worse than a simple two-category model with a constant ice strength parameter P (Ungermann et al., 2017). It was also recently presented that plastic-like rheologies must be run at high resolution (about 0.5-1 km) to be able to simulate some localization of the sea ice deformation at 10 km (Hutter et al., 2017). In light of the scaling laws of sea ice deformation, the redistribution schemes should also be scale-dependent and take into account the spatial and temporal scale at which the deformation is represented in the given large-scale model. Even the promising Maxwell-Elasto-Brittle approach is not complete because it lacks an energy-consistent formulation to link the energy dissipated by viscous relaxation to the ridging scheme.

However, it is now thought that a consistent modelling framework can be built to reproduce adequately sea ice deformation across a wide range of scales. At least we have now all the ingredients. The framework presented here also brings a parallel with ocean models, as we could classify the sea ice models into three categories:

1. Large-scale circulation models that correctly simulate the mean circulation at typical scales of hundreds of kilometers and hundreds of days.

2. Lead/ridge-permitting models that allow the strain localization when they run at resolutions between 0.1 and 100 km and reproduce the scaling laws from their temporal and spatial resolution up to cutting scales of 100 km and ten days.
3. Lead/ridge/floes resolving models that run at resolution of the order of 1 m and that explicitly represent individual ridges, leads, and floes.

Some may extrapolate and suggest that lead/ridge permitting continuous models could be used to simulate explicitly the deformation at the scale of one ridge/lead/floe, but this is probably unrealistic as the assumptions (i.e., two-dimensional and isostatic assumptions) made to build a continuous sea ice model are surely not valid for a resolution higher than about 100 m. This would be equivalent to suggesting that hydrostatic hydrodynamic models could explicitly reproduce non-hydrostatic flows.

Lead permitting models and impacts on the ocean-atmosphere interactions

When a lead opens in the ice during winter, relatively warm ocean waters are exposed to the cold atmosphere resulting in heat fluxes of up to 600 W/m^2 (e.g., Maykut, 1986; Andreas and Murphy, 1986). As a result, a plume of warm, moist air forms over the lead, sometimes resulting in ice fog, which significantly reduces visibility and can cause ice to accumulate on surfaces such as aircraft, power lines, and roads (e.g., Gultepe et al., 2015). This release of heat also causes convection in the predominantly stable or near-neutral Arctic atmospheric boundary layer, and as the plume rises it may penetrate the lowest levels of the capping inversion, leading to entrainment (see Lupkes et al., 2008a; 2008b; Vihma et al., 2013 for an overview). On the oceanic side, ice forming in leads removes fresh water from the ocean and releases brine (e.g., Smith et al., 1974; Kozo, 1983; Morrison et al., 1992). The brine plumes spread horizontally along the top of the halocline, reducing the depth of the mixed layer, but they do not penetrate the halocline. Nguyen et al. (2009), using subgrid-scale parameterization of brine rejection, showed that a faithful simulation of the Arctic halocline depends on the proper representation of brine release and its redistribution in the water column.

Before analyzing such processes in coupled ice-ocean-(atmosphere) systems, one should determine how well the leads are represented by the sea ice model. In this section, we recap the results of Olason et al. (2017), who performed such an analysis by comparing statistically observed lead fraction data to lead fraction simulated by the neXtSIM model described previously. We show that the model reproduces the spatial scaling of the lead fraction statistics down to its resolution, indicating that the model is “lead permitting.”

Observations of lead fraction can be derived from passive microwave observations of the AMSR-E (the Advanced Microwave Scanning Radiometer for EOS). For example, the dataset produced by Ivanova et al. (2016) is available on a daily basis for the Arctic region from November to April, from 2002 to 2011. The dataset resolution is 6.25 km and the method allows leads wider than 3 km to be detected, meaning that a substantial amount of smaller leads is undetected in this product. The data show the area fraction of each grid cell covered by leads that are filled with open water and thin ice (see Fig. 15.9).

We use the latest version of the next generation sea ice model, neXtSIM, described earlier. The model uses the Maxwell-Elasto-Brittle rheology of Dansereau et al. (2016), a Lagrangian moving mesh as described in Rampal et al. (2016a), and the thermodynamic growth is modelled using the two-layer model of Winton (2000). The model has three ice categories, thick ice, open water, and newly formed thin ice. The model set-up covers the Central Arctic Ocean, with open boundaries at the Bering Strait and through the Canadian Arctic Archipelago, Greenland, Barents, and Kara Seas. The model is forced using daily mean results from the TOPAZ4 oceanic reanalysis (Sakov et al., 2012) and 6-hourly results from the CFSR and CFSv2 atmospheric reanalysis (Suranjana et al., 2010; 2012).

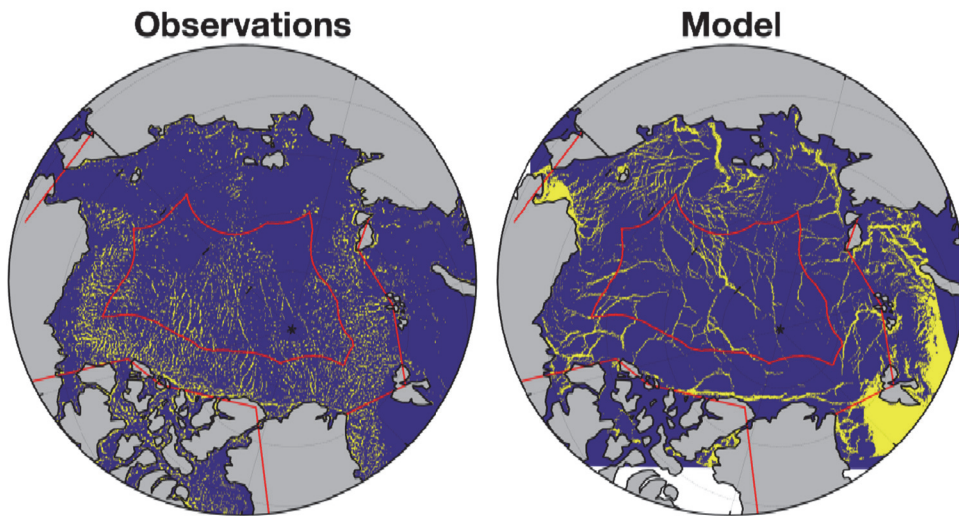


Figure 15.9. Observed and simulated leads on January 1, 2011. The figure shows the entire model domain, and the red lines indicate the boundaries of the “Arctic” (outer region) and “Central Arctic” regions used in the study. Lead fraction larger than 0.01 is indicated in yellow. Figure from Ólason et al. (2017).

As shown in Fig. 15.9, the model produces highly localized lead fraction as in the observations. The lead density is somewhat weaker than in the observations, especially in the Beaufort Sea and north of the Fram Strait; this issue is still under investigation. As for the deformation, we can explore the spatial scaling of the lead fraction simulated by the model. Due to the presence of large coastal and flaw polynyas, we confine the analysis to the Central Arctic (more than 400 km away from the coast). The results of this analysis can be seen in Fig. 15.10, which shows a clear scaling of the lead fraction statistics with a spatial scale that is similar to the one obtained from other observations (not shown here). When conducting the same analysis for simulations run at coarser resolutions, respectively 10 and 20 km, the scaling still holds down to the model resolution, meaning that the model localizes the deformation (and thus the lead fraction) down to its resolution.

There is certainly room for improvement, but the fact that the model reproduces the scaling laws of the lead fraction statistics down to its resolution means that it provides the correct estimate of the heterogeneity of that field at that scale. Subgrid-scale parameterizations are still needed to connect with the scale of the leads, and this could be accomplished based on the observed or simulated scaling laws. The best platform to investigate the effects of the better representation of the lead

fraction on the heat fluxes is, of course, a coupled ice-ocean-atmosphere model that allows us to simulate the feedbacks between the localization of lead fraction, the heat fluxes, and the effects on the ocean and atmosphere.

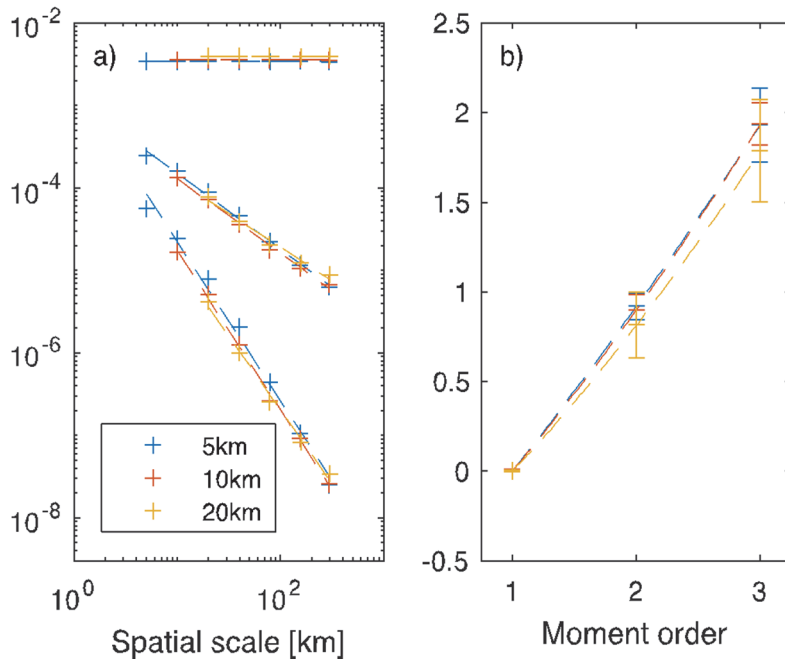


Figure 15.10. The spatial scaling of modelled lead fraction in the “Central Arctic” region over JFM, 2011. The colours denote results from runs at different model resolutions. The left panel shows the mean, variance, and skewness of the lead fraction as a function of the scale of observation. The dashed lines are linear fits for each moment. The right panel shows the slope of the scaling as a function of the moment order ($q=1$ for the mean, $q=2$ for the variance and $q=3$ for the skewness). Figure from Ólason et al. (2017).

New Frontiers in Sea Ice Forecasting

To operate in ice-infested water (e.g., shipping, scientific campaigns) depends heavily on local weather and sea ice conditions (see Eicken, 2013; Riska and Coche, 2013). Building forecast systems capable of reproducing and predicting local ice conditions would complement the currently available forecasting services based on ice charts, large-scale forecasts, and satellite images.

When building a forecast system, one must first determine what the users need. For example, most captains navigating close to or in the ice pack use information from daily ice charts. The ice charts define areas of different classes of ice concentration, types, and thicknesses. They also often use synthetic-aperture radar or visible satellite images where fine structures such as leads and ridges can be fairly well identified by trained sea ice experts. Therefore, systems able to provide this type of information several days in advance with enough confidence would be very valuable. Forecast systems can also provide information that does not exist in ice charts and synthetic-aperture radar images, especially the information on the sea ice drift and deformation. Such information is crucial

when determining if a ship will be trapped in a converging zone, or to assist search and rescue operations in case of an incident or oil spill, for example.

The term “forecasting” is also used for seasonal and decadal predictions that aim to predicting the intra-annual and inter-annual large-scale variations of the ice pack state (total extent, volume, ...). Although not discussed in detail here, it is worth noting that this research activity has potentially large economical and societal impacts.

Operational sea ice forecasting is relatively new compared to weather and ocean operational forecasting. Initially, the sea ice forecaster community decided to apply data assimilation methods developed for the atmosphere and ocean to the sea ice. However, this strategy may not be optimal for the following reasons:

1. Data for sea ice are mainly derived from satellite products that have good coverage but potentially systematic biases as well as random noise.
2. Most sea ice forecast systems are open system forced by external forcing from ocean and/or atmosphere models, with potential time varying biases.
3. Sea ice dynamics is often far from equilibrium and characterized by large discontinuities in space and time.

In this section we present two examples where these three points are discussed. In the first, we will try to answer the question: “How can we beat ice charts persistency?” and we will discuss the use of (1) potentially biased data and (2) potentially biased forcing. Next, we will ask the question: “How can we forecast local-scale deformation and drift several days in advance?” and we will discuss data assimilation for systems that are far from dynamical equilibrium, i.e., sub-critical. In each case, we present observations, data assimilation methods, and model components that could be used in an operational system to achieve those objectives. The list of observations, assimilation methods, and model components presented here is not exhaustive and does not especially correspond to what is used today in sea ice forecasting. For such a review, please refer to the book: *Sea ice analysis and forecasting* (2017).

Can we beat ice charts persistency?

Most of the operators working in ice-infested waters rely on near real-time data acquired from satellites and distributed directly as synthetic-aperture radar images or indirectly as ice charts. One way to convince these “clients” to use model forecast outputs is to show *a posteriori* that the information we were able to provide for a given time t is in better agreement with the corresponding information observed during those days than the information available at time t . In other words, we have to prove that we are able to surpass the persistency of their preferred source of near real-time data.

Forecasting synthetic-aperture radar-like data is still a futuristic concept, as one would need to use very high-resolution systems (of the order of 10 m). On the other hand, forecasting ice charts-like maps could be achieved using existing systems. Ice charts usually cover regional or Arctic-wide domains and provide, on a daily basis, information on the ice concentration from the day

before. The production of ice charts is made by sea ice analysts who combine data from various sources (synthetic-aperture radar images, passive microwave satellite data, in situ observations, forecast systems, etc.) in order to provide maps of ice classes.

Typically, operational sea ice forecasts are not based on ice charts but directly on passive microwave satellite data, providing daily estimates of sea ice concentration at resolution of about 5-20 km. However, it is important to note that these data are indirect measurements of sea ice concentration and are subject to well-known biases. They usually perform badly when ice ponds are present, for thin ice, for highly fragmented and low concentration ice, and near the ice edge. Building a system taking all these limitations into account is feasible, but has not yet been achieved. Another solution is to directly assimilate ice charts that are also provided on a daily basis and are known to have less persistent bias.

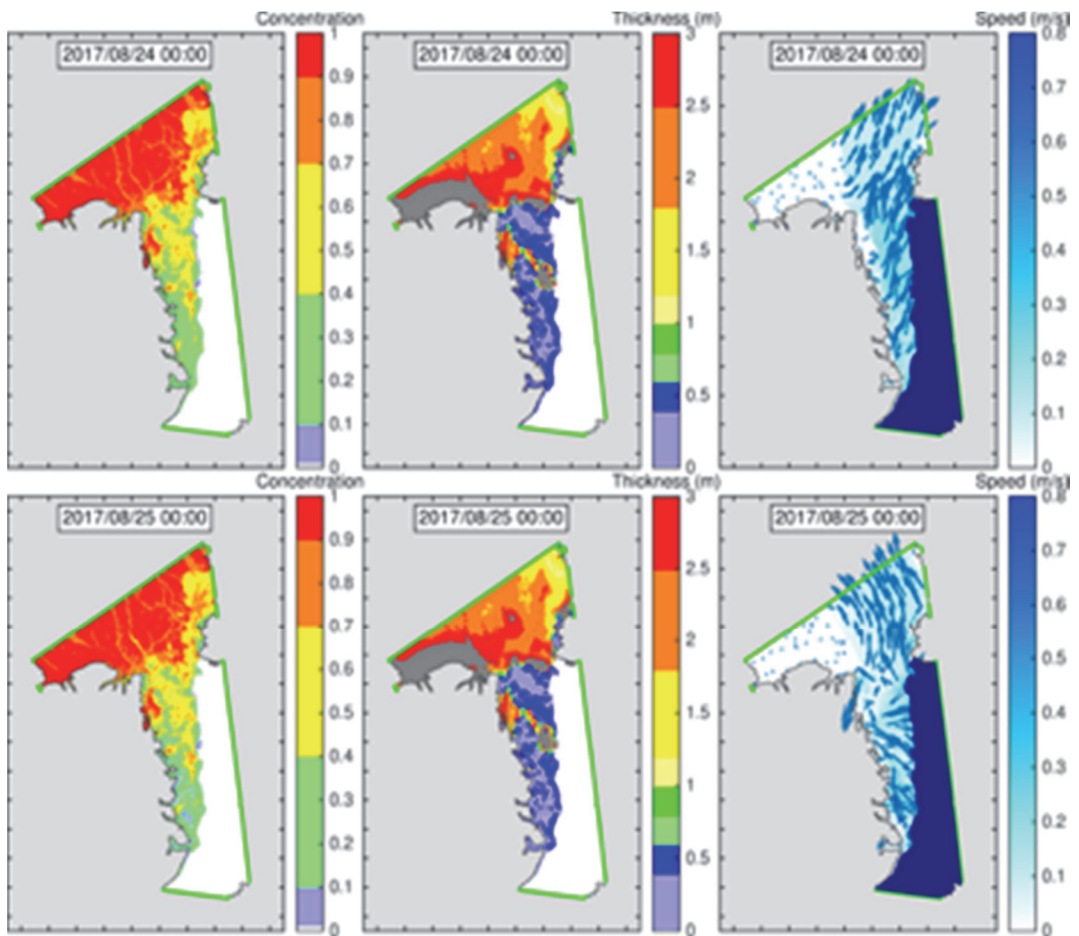


Figure 15.11. Examples of sea ice concentration, thickness and velocity forecasted by the neXtSIM-F setup for the Greenland Sea and Fram Strait for the T+24h (top panel) and T+48h (bottom panel) time horizons in August 2017. Plotted ice drift vectors are instantaneous drift at noon of that day. The concentration maps use the color code from the Norwegian ice charts and show five different ice classes. The ice thickness maps use eight different classes that matches with the ice breaker classification of Bureau Veritas.

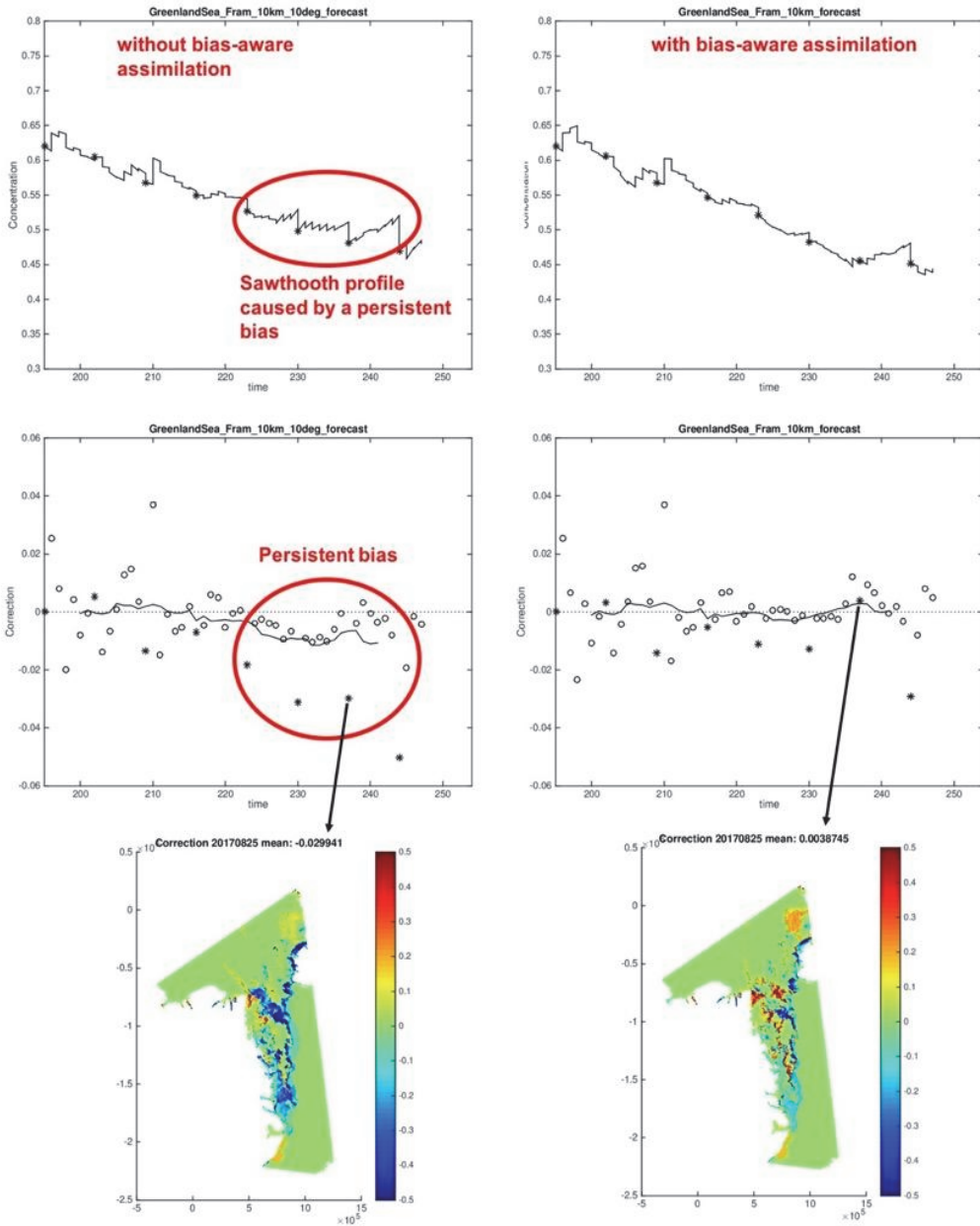


Figure 15.12. Comparison of a reforecast simulation starting on July 14, 2017 and running until September 04, 2017 (days 194 to 247), with the default data assimilation system (left) and the bias-aware assimilation system (right). The first row shows the total concentration (total area of ice divided by the area of the domain). The stars indicate when the weekly U.S. National Ice Center ice charts are assimilated (every Friday). The second row shows the mean update for the ice concentration. The third row shows an example of the concentration update field for August 25, 2017.

The neXtSIM-F is an experimental sea ice forecast platform based on the neXtSIM sea ice model (Bouillon and Rampal, 2015; Rampal et al., 2016a; 2016b; Rampal et al. 2017) and on the assimilation of multiple satellite-derived operational products and ice charts. The set-up presented here covers the Greenland Sea and Fram Strait and provides a seven-day sea ice forecast at a resolution of 10 km on a daily basis (see Fig. 15.11). The initial forecast conditions are computed by assimilating sea ice concentration from the daily and weekly ice charts produced by the U.S. National Ice Center into the model state as given by the previous forecast. The model is forced with the deterministic atmosphere forecast from the European Centre for Medium-Range Weather Forecasts and the ocean forecast is from the Arctic – Monitoring Forecasting Centre.

We implement a sequential and intermittent bias-aware assimilation scheme where the model state is modified towards observations every day. This correction step helps to start the forecast with conditions that are consistent with observations (here, the U.S. National Ice Center daily and weekly ice charts); this also helps to detect and correct biases in the model parameters or in the forcing. The daily U.S. National Ice Center ice charts contain three categories for ice concentration: below 0.1, between 0.1 and 0.8, and between 0.8 and 1 (see http://www.natice.noaa.gov/daily_graphics.htm). The weekly ice charts contain many more categories, typically [no ice, 0-0.1, 0.1-0.4, 0.4-0.6, 0.6-0.8, 0.8-1, 1].

The control parameter for the bias-aware data assimilation is defined here as a correction term applied to the near surface air temperature taken by the European Centre for Medium-Range Weather Forecasts' atmospheric forecast. In the control run, without bias-aware assimilation (Fig. 15.12, left panels), we set this correction constant and equal to -10°C , which is a value that was fitted manually from preliminary tests. When the bias-aware assimilation is activated (Fig. 15.12, right panels), the correction term is updated every day from the analysis of two additional one-day runs using a correction equals to $+ \text{ or } - 10^{\circ}\text{C}$, respectively. In the case presented here, the correction starts from the default value (-10°C) and varies smoothly between -15 and 0°C .

Can we forecast local-scale deformation days in advance?

Data assimilation methods are classically ranked from the most rudimentary direct insertion to advanced Ensemble Kalman Filtering (EnKF) and 4-D variational methods. Direct insertion applies the observations directly into the corresponding model variables, but should only be used if all the model prognostic variables are observed; it then honors perfectly the assimilated observations. However, when different observation types may be inconsistent, their uncertainty levels must be taken into account; this can be done by optimal interpolation. The EnKF and 4D-Var are able to project information from observed to unobserved model variables, and are also able to assimilate observations of different types. We argue that advanced data assimilation methods are not necessary for a stand-alone sea ice forecasting model and that better forecast performance can be attained using rudimentary methods.

Sea ice deformation simulated with the neXtSIM model spontaneously localizes along linear-like faults, separating essentially undamaged ice plates/floes. Modelled faults are transient features, accommodating permanent sea ice deformation for awhile before ceasing their activity depending

on the refreezing kinetics, the evolution of the wind forcing, and the internal sea ice dynamics, as observed from satellite imagery.

By initializing the model damage variable using past observations of sea ice deformation, we can transfer crucial information to the forecasting system on the history of the deformation that is likely to improve its predictive skill (see Fig. 15.13). The assimilation of information on past shear deformation (and potentially on lead fraction) allows for simulating sea ice drift and its gradient with high accuracy.

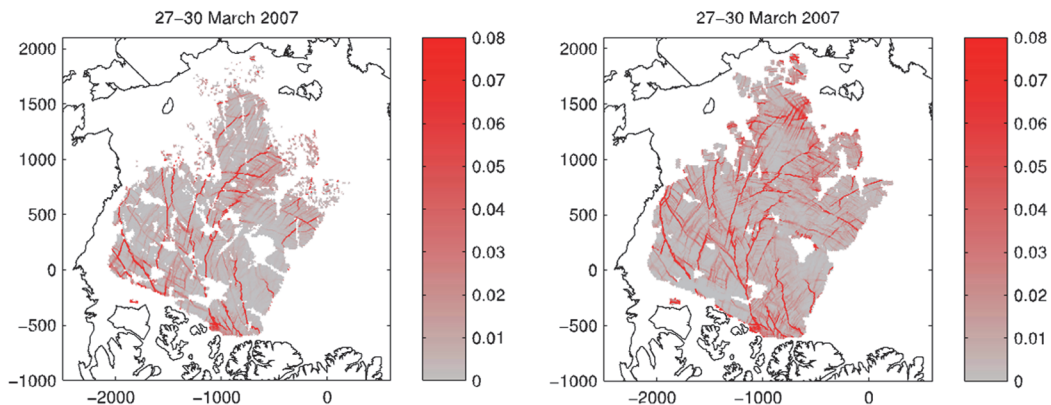


Figure 15.13. Preliminary results illustrating the potential of assimilating information on observed sea ice deformation through the damage variable in the neXtSIM model. The figure shows the observed (left) and simulated (right) shear rate for the same area and for a period centered on March 27–30, 2007. The simulation began on March 26, with a damage field initialized using the deformation rate shown on the left panel and which is computed from synthetic-aperture radar observations.

Conclusion

This chapter about new frontiers in sea ice modelling and forecasting focused on the representation of sea ice dynamics in continuous sea ice models. First, we described the complexity of ice pack dynamics and its underlying causes, defined a framework to discuss the degree of complexity of sea ice models as a function of their ability to resolve fine dynamical structures, and illustrated the potential impact of using lead-permitting continuous sea ice model in coupled systems. Next, in the section on sea ice forecasting, we presented two examples of specific data assimilation issues related to sea ice modelling. This included a solution to tackle the problem of persistent biases in the observations and external forcing and a proposition to use near real-time deformation data to better constraint sea ice forecast initial state and thus be able to forecast accurately sea ice drift and deformation.

Our overall conclusion is that sea ice remains fascinating, even for scientists having worked on the topic for years. There are still many unanswered questions, especially related to the impacts of better resolving sea ice dynamics in coupled ice-ocean-atmosphere systems. We hope that our participation in the GODAE school inspired some of the attendees to join us in investigating these issues.

References

- Aagaard, Coachman, Carmack. 1981: On the halocline of the Arctic Ocean, *Deep Sea Research Part A. Oceanographic Research Papers*, 28, 529 – 545, doi:10.1016/0198-0149(81)90115-1.
- Andreas, Murphy. 1986: Bulk transfer coefficients for heat and momentum over leads and polynyas, *J. Phys. Ocean.*, 16, 1875–1883.
- Andreas, Cash. 1999: Convective heat transfer over wintertime leads and polynyas, *Journal of Geophysical Research: Oceans*, 104, 25721–25734, doi:10.1029/1999JC900241, <http://dx.doi.org/10.1029/1999JC900241>.
- Andreas, Paulson, William, Lindsay, Businger. 1979: The turbulent heat flux from arctic leads, *Boundary-Layer Meteorology*, 17, 57–91, doi:10.1007/BF00121937.
- Bazant. 2000: "Scaling laws for brittle failure of sea ice." Preprints, IUTAM Symp. on Scaling Laws in Ice Mechanics (Univ. of Alaska, Fairbanks, June), J.P. Dempsey, H.H. Shen and L.H. Shapiro, eds. Paper No.3, pp. 1-23.
- Bouillon, Rampal. 2015: Presentation of the dynamical core of neXtSIM, a new sea ice model, *Ocean Modelling*, 91(C), 23–37, doi:10.1016/j.ocemod.2015.04.005.
- Bouillon, Rampal. 2015a: On producing sea ice deformation data sets from SAR-derived sea ice motion, *The Cryosphere*, 9(2), 663–673, doi:10.5194/tc-9-663-2015.
- Dansereau, Weiss, Saramito, Lattes. 2016: A Maxwell elasto-brittle rheology for sea ice modelling, *The Cryosphere*, 10, 1339–1359, doi:10.5194/tc-10-1339-2016, <https://www.the-cryosphere.net/10/1339/2016/>
- Eicken. 2013: Ocean science: Arctic sea ice needs better forecasts. *Nature*, 497(7450), 431–433, doi:10.1038/497431a.
- Gultepe, Zhou, Milbrandt, Bott, Li, Heymsfield, Ferrier, Ware, Pavolonis, Kuhn, Gurka, Liu, Cermak. 2015: A review on ice fog measurements and modeling, *Atmospheric Research*, 151, 2 – 19, doi:10.1016/j.atmosres.2014.04.014, sixth International Conference on Fog, Fog Collection and Dew.
- Hebert, Allard, Metzger, Posey, Preller, Wallcraft, Phelps, Smedstad. 2015: Short-term sea ice forecasting: An assessment of ice concentration and ice drift forecasts using the U.S. Navy's Arctic Cap Nowcast/Forecast System, *J. Geophys. Res.*, 120, 8327–8345, doi:10.1002/2015JC011283.
- Hibler. 1979: A dynamic thermodynamic sea ice model. *J. Phys. Oceanogr.*, 9, 815–846, doi:10.1175/1520-0485(1979)009<0815:ADTSIM>2.0.CO;2.
- Hopkins, Hibler, Flato. 1991b: On the numerical simulations of the sea ice ridging process. *J. Geophysical Res.* 96(C3): 4809-4820.
- Hutchings, Hibler. 2008: Small-scale sea ice deformation in the Beaufort Sea seasonal ice zone, *J. Geophys. Res. Oceans*, 113, doi:10.1029/2006JC003971.
- Hutchings, Roberts, Geiger, Richter-Menge. 2011: Spatial and temporal characterization of sea-ice deformation, *Ann. Glac.*, 2011, 52, 360–368, doi:10.3189/172756411795931769.
- Hutter, Losch, Menemenlis. 2017: Scaling properties of Arctic sea ice deformation in high-resolution viscous-plastic sea ice models and satellite observations, European Geosciences Union General Assembly 2017, Vienna, 23 April 2017 - 28 April 2017.
- Ivanova, Rampal, Bouillon. 2016: Error assessment of satellite-derived lead fraction in the Arctic, *The Cryosphere*, 10, 585–595, doi:10.5194/tc-10-585-2016, <https://www.the-cryosphere.net/10/585/2016>.
- Kozo. 1983: Initial model results for Arctic mixed layer circulation under a refreezing lead, *Journal of Geophysical Research: Oceans*, 88, 2926–2934, doi:10.1029/JC088iC05p02926, <http://dx.doi.org/10.1029/JC088iC05p02926>.
- Kwok, Curlander, McConnell, Pang. 1990: An Ice Motion Tracking System at the Alaska SAR Facility, *IEEE J. of Oceanic Engineering*, 15, 44–54.
- Kwok. 2001: Deformation of the Arctic Ocean Sea Ice Cover between November 1996 and April 1997: A Qualitative Survey. In: Dempsey J.P., Shen H.H. (eds) IUTAM Symposium on Scaling Laws in Ice Mechanics and Ice Dynamics. Solid Mechanics and Its Applications, vol 94. Springer, Dordrecht.
- Lüpkes, Gryanik, Witha, Gryschka, Raasch, Gollnik. 2008a: Modeling convection over arctic leads with LES and a non-eddy-resolving microscale model, *J. Geophys. Res.*, 113, C09 028, doi:10.1029/2007JC004099.
- Lüpkes, Vihma, Birnbaum, Wacker. 2008b: Influence of leads in sea ice on the temperature of the atmospheric boundary layer during polar night, *Geophys. Res. Lett.*, 35, doi:10.1029/2007GL032461.
- Marcq, Weiss. 2012: Influence of sea ice lead-width distribution on turbulent heat transfer between the ocean and the atmosphere, *The Cryosphere*, Volume 6, Issue 1, 2012, pp. 143-156, 6, 143–156.
- Marsan, Stern, Lindsay, Weiss. 2004: Scale Dependence and Localization of the Deformation of Arctic Sea Ice, *Phys. Rev. Lett.*, 93, 178501, doi:10.1103/PhysRevLett.93.178501.

- Maykut. 1986: The surface heat and mass balance, in: *The Geophysics of Sea Ice*, edited by Untersteiner, N., NATO ASI Series, chap. 5, pp. 395–463, Springer US.
- Nguyen, Menemenlis, Kwok. 2009: Improved modeling of the Arctic halocline with a subgrid-scale brine rejection parameterization, *Journal of Geophysical Research: Oceans*, 114, n/a–n/a, doi:10.1029/2008JC005121, <http://dx.doi.org/10.1029/2008JC005121>, c11014.
- Ólason, Rampal, Bouillon. 2017: On the statistical properties of sea ice lead fraction and heat fluxes in Arctic, submitted to *The Cryosphere*.
- Rampal, Weiss, Marsan. 2009: Positive trend in the mean speed and deformation rate of Arctic sea ice, 1979–2007, *J. Geophys. Res.*, 114(C5), C05013, doi:10.1029/2008JC005066.
- Rampal, Bouillon, Ólason, Morlighem. 2016: neXtSIM: a new Lagrangian sea ice model, *The Cryosphere*, 10, 1055–1073, doi:10.5194/tc-10-1055-2016, <http://www.the-cryosphere.net/10/1055/2016/>.
- Rampal, Bouillon, Ólason, Dansereau, Williams, Samaké. 2017: On the simulation of scaling properties of sea ice deformation, submitted to *The Cryosphere*.
- Riska, Coche. 2013: Station keeping in ice - challenges and possibilities, Proceedings of the 22nd International Conference on Port and Ocean Eng under Arctic Conditions (POAC), June 9-13, Espoo, Finland.
- Samaké, Bouillon, Rampal, Ólason. 2017: Parallel Implementation of a Lagrangian-based Model on an Adaptive Mesh in C++: Application to Sea-Ice. *Journal of Computational Physics*, dx.doi.org/10.1016/j.jcp.2017.08.055
- Schweiger, Zhang. 2015: Accuracy of short-term sea ice drift forecasts using a coupled ice-ocean model, *J. Geophys. Res.*, 120, doi:10.1002/2015JC011273.
- Thorndike, Rothrock, Colony. 1975: The thickness distribution of sea ice. *J. Geophys. Res.: Oceans*, 80(33), 4501–4513.
- Vihma, Pirazzini, Renfrew, Sedlar, Tjernström, Nygård, Fer, Lüpkes, Notz, Weiss, Marsan, Cheng, Birnbaum, Gerland, Chechin, Gascard. 2013: Advances in understanding and parameterization of small-scale physical processes in the marine Arctic climate system: a review, *Atmos. Chem. Phys. Discuss.*, 13, 32 703–32 816.
- Weeks. 2010: *On sea ice*, University of Alaska Press, Fairbanks. ISBN 978-1-60223-079-8. *Geol. J.*, 46: 657. doi:10.1002/gj.1285.
- Weiss, Schulson, Stern. 2007: Sea ice rheology from in-situ, satellite and laboratory observations: Fracture and friction. *Earth and Planetary Science Letters*, 255(1-2), 1–8. <http://doi.org/10.1016/j.epsl.2006.11.033>
- Weiss. 2013: *Drift, deformation and fracture of sea ice - A perspective across scales*, Springer, Dordrecht, The Netherlands, doi:10.1007/978-94-007-6202-2.
- Winton. 2000: A reformulated three-layer sea ice model, *J. Atm. Ocean. Tech.*, 17, 525–531.

